Inhomogeneity and variability of the spectral index in flaring sources observed by STIX

Università di Genova
DIMA | Dipartimento di Matematica

Anna Volpara, Paolo Massa, Andrea Francesco Battaglia,
Säm Krucker, Gordon Hurford, Michele Piana, Anna Maria Massone

STIX team meeting
April 11, 2023

Outline

1. From photon to electron visibilities
2. Visibility inversion algorithm
3. Results
4. Conclusions and future works

From photon to electron visibilities

Photon visibilities:

$$V(u,v;\epsilon) = \mathcal{F}(I(x,y;\epsilon)) = \int\int I(x,y;\epsilon) e^{2\pi i(xu+yv)}\, dx\, dy \qquad (1)$$

From photon to electron visibilities

Photon visibilities:

$$V(u,v;\epsilon) = \mathcal{F}(I(x,y;\epsilon)) = \int\int I(x,y;\epsilon) e^{2\pi i(xu+yv)}\, dx\, dy \qquad (1)$$

Intensity of the X-ray photon flux emitted from (x, y) on the Sun

From photon to electron visibilities

Photon visibilities:

$$V(u,v;\epsilon) = \mathcal{F}(I(x,y;\epsilon)) = \int\int I(x,y;\epsilon) e^{2\pi i(xu+yv)}\, dx\, dy \qquad (1)$$

Array containing the N_V complex values of the visibilities measured by STIX

From photon to electron visibilities

Photon visibilities:

$$V(u,v;\epsilon) = \mathcal{F}(I(x,y;\epsilon)) = \int\int I(x,y;\epsilon) e^{2\pi i(xu+yv)}\, dx\, dy \qquad (1)$$

The Fourier Transform

From photon to electron visibilities

Photon visibilities:

$$V(u,v;\epsilon) = \mathcal{F}(I(x,y;\epsilon)) = \int\int I(x,y;\epsilon) e^{2\pi i(xu+yv)}\, dx\, dy \tag{1}$$

Bremsstralhung equation:

$$I(x,y;\epsilon) = \frac{a}{4\pi R^2} \int_{\epsilon}^{\infty} N(x,y)\bar{F}(x,y,E)Q(\epsilon,E)\, dE \tag{2}$$

$$N(x,y) = \int_0^{\ell(x,y)} n(x,y,z)\, dz$$

$n(x,y,z)$ is the local density of target particles along the line-of-sight depth $\ell(x,y)$

$$\bar{F}(x,y;E) = \frac{1}{N(x,y)} \int_0^{\ell(x,y)} n(x,y,z) F(x,y,z;E)\, dz$$

$F(x,y,z;E)$ is the differential electron flux spectrum at the point (x,y,z)

From photon to electron visibilities

Photon visibilities:

$$V(u,v;\epsilon) = \mathcal{F}(I(x,y;\epsilon)) = \int\int I(x,y;\epsilon) e^{2\pi i(xu+yv)}\, dx\, dy \tag{1}$$

Bremsstralhung equation:

$$I(x,y;\epsilon) = \frac{a}{4\pi R^2} \int_{\epsilon}^{\infty} N(x,y)\bar{F}(x,y,E)Q(\epsilon,E)\, dE \tag{2}$$

Electron visibilities:

$$W(u,v,E) = \frac{a}{4\pi R^2} \int\int N(x,y)\bar{F}(x,y;E) e^{2\pi i(xu+yv)}\, dx\, dy \tag{3}$$

Bremsstralhung equation for visibilities:

$$V(u,v;\epsilon) = \int_{\epsilon}^{\infty} W(u,v;E)Q(\epsilon,E)\, dE \tag{4}$$

Measured photon visibilities

Electron visibilities

Visibility inversion algorithm - Photon visibilities

Photon visibilities

$$
\begin{array}{c|cccc}
 & \varepsilon_1 & \varepsilon_2 & \cdots\cdots & \varepsilon_N \\
(u_1, v_1) & V_{1,1} & V_{1,2} & \cdots\cdots & V_{1,N} \\
(u_2, v_2) & V_{2,1} & V_{2,2} & \cdots\cdots & V_{2,N} \\
\vdots & \vdots & \vdots & \ddots & \vdots \\
(u_{N_V}, v_{N_V}) & V_{N_V,1} & V_{N_V,2} & \cdots\cdots & V_{N_V,N}
\end{array}
$$

Visibility inversion algorithm - Photon visibilities

Photon visibilities

$$
\begin{array}{c|cccc}
 & \varepsilon_1 & \varepsilon_2 & \cdots\cdots & \varepsilon_N \\
(u_1, v_1) & V_{1,1} & V_{1,2} & \cdots\cdots & V_{1,N} \\
(u_2, v_2) & V_{2,1} & V_{2,2} & \cdots\cdots & V_{2,N} \\
\vdots & \vdots & \vdots & \ddots & \vdots \\
(u_{N_V}, v_{N_V}) & V_{N_V,1} & V_{N_V,2} & \cdots\cdots & V_{N_V,N}
\end{array}
$$

May 7, 2021 – 18:51 UT

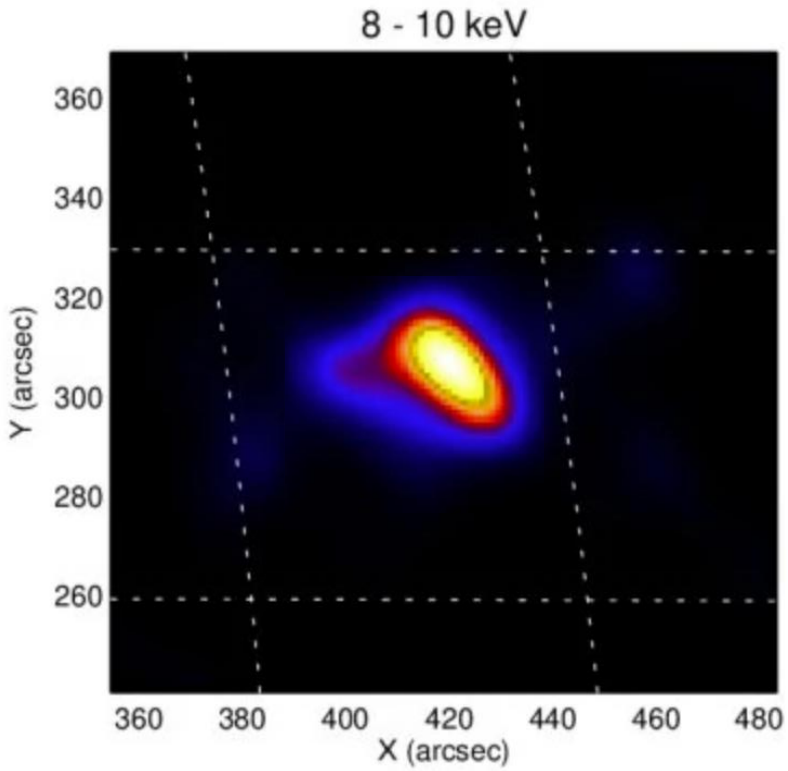

Reconstruction provided by MEM_GE, from photon visibilities.

Visibility inversion algorithm - Photon visibilities

Photon visibilities

$$
\begin{array}{c|cccc}
 & \varepsilon_1 & \varepsilon_2 & \cdots\cdots & \varepsilon_N \\
(u_1, v_1) & V_{1,1} & V_{1,2} & \cdots\cdots & V_{1,N} \\
(u_2, v_2) & V_{2,1} & V_{2,2} & \cdots\cdots & V_{2,N} \\
\vdots & \vdots & \vdots & \ddots & \vdots \\
(u_{N_V}, v_{N_V}) & V_{N_V,1} & V_{N_V,2} & \cdots\cdots & V_{N_V,N}
\end{array}
$$

May 7, 2021 – 18:51 UT

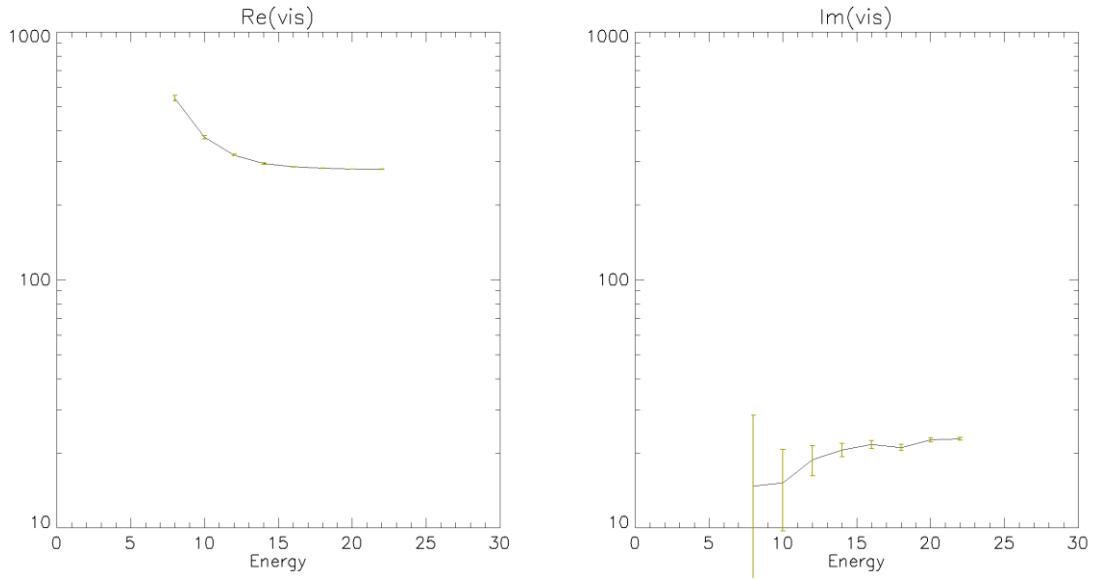

Real part (*on the left*) and imaginary part (*on the right*) of observed photon visibilities in $(u, v) = (0.002, -0.001)$ considering eight energy bands ($N = 8$).

Electron visibilities

Electron visibilities

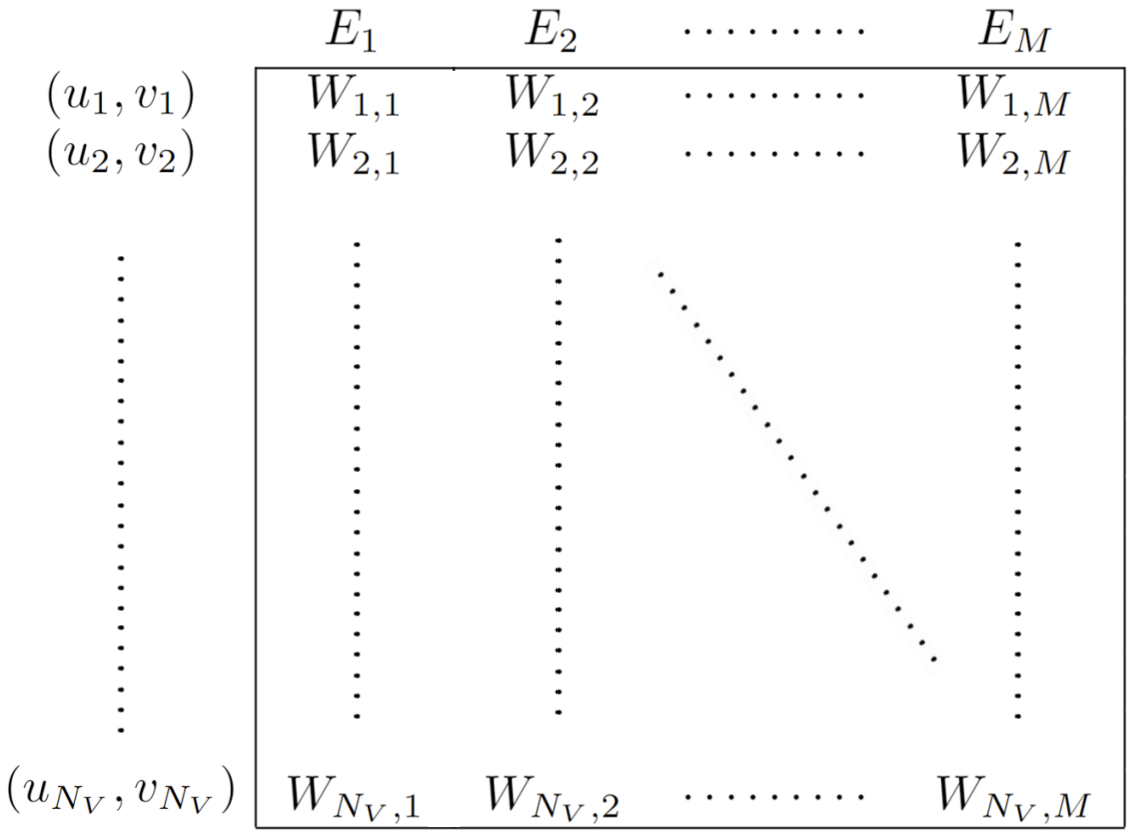

Electron visibilities

Electron visibilities

$$
\begin{array}{c|cccc}
 & E_1 & E_2 & \cdots\cdots & E_M \\
(u_1, v_1) & W_{1,1} & W_{1,2} & \cdots\cdots & W_{1,M} \\
(u_2, v_2) & W_{2,1} & W_{2,2} & \cdots\cdots & W_{2,M} \\
\vdots & \vdots & \vdots & \ddots & \vdots \\
(u_{N_V}, v_{N_V}) & W_{N_V,1} & W_{N_V,2} & \cdots\cdots & W_{N_V,M}
\end{array}
$$

May 7, 2021 – 18:51 UT

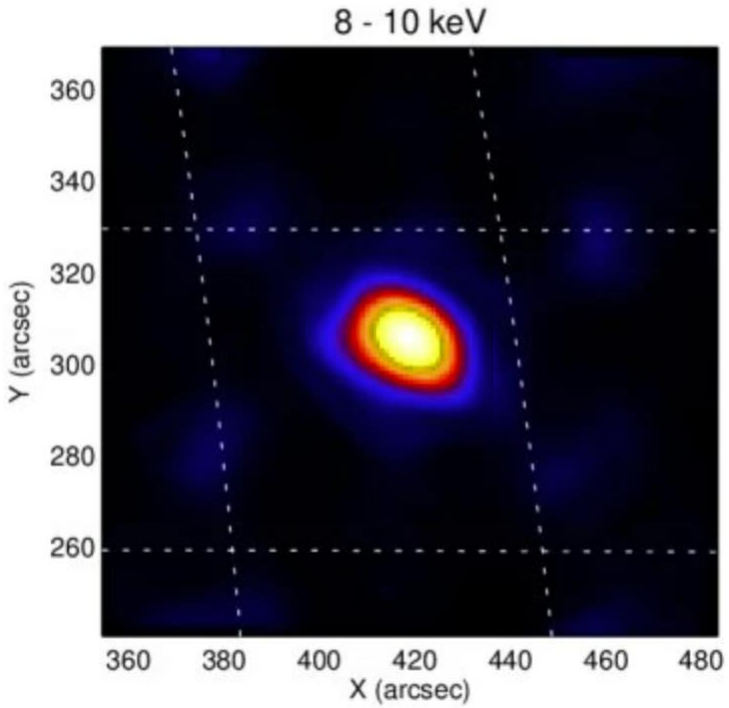

Reconstruction provided by MEM_GE, from electron visibilities.

Results – May 7, 2021

Photon images

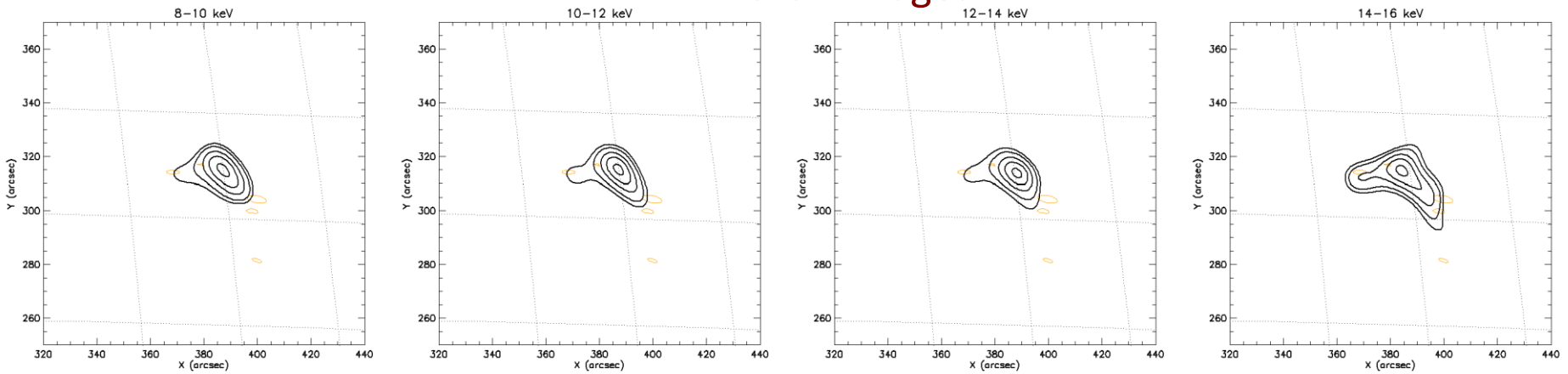

Electron flux images

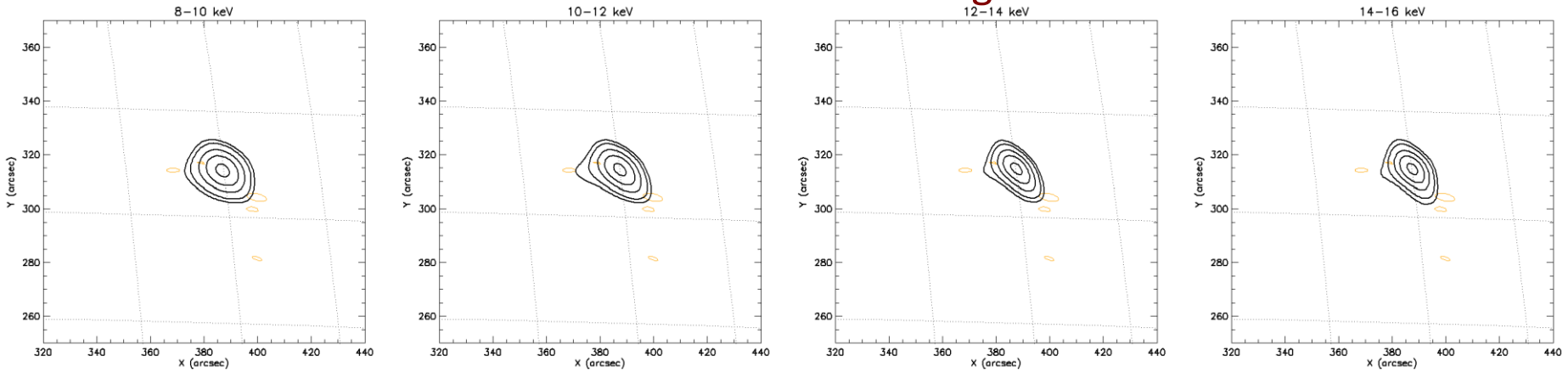

Photon images for the energy intervals shown (*top panels*), compared with the electron flux images corresponding to the regularized electron visibilities (*bottom panels*) in the same energy range. The 50% contour levels of the AIA images are plotted in orange, while the 25, 35, 55, 75, 95% contour levels of the reconstructed map are plotted in black. The maps are produced using the MEM-GE algorithm.

Results – May 7, 2021

Photon images

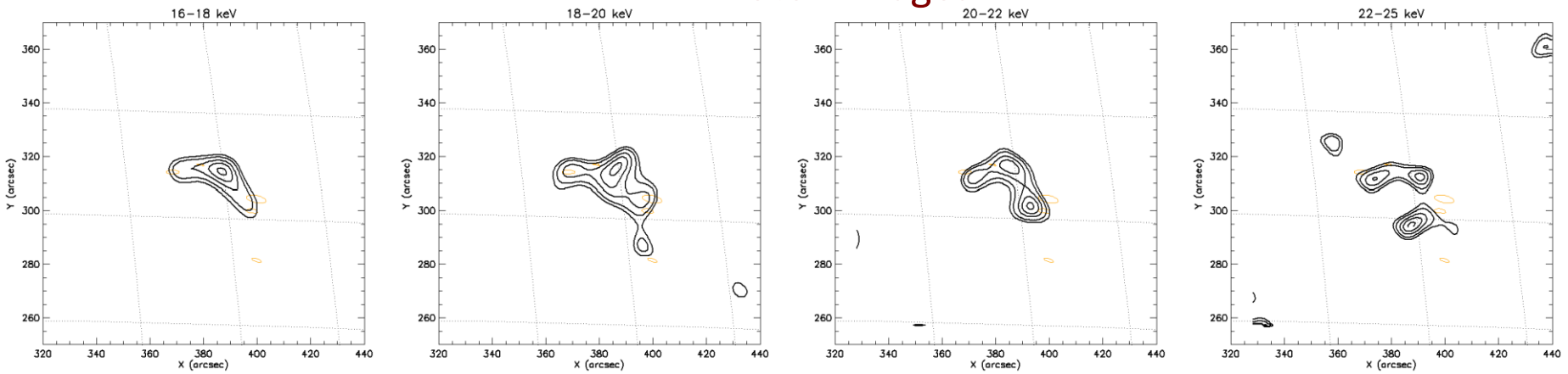

Electron flux images

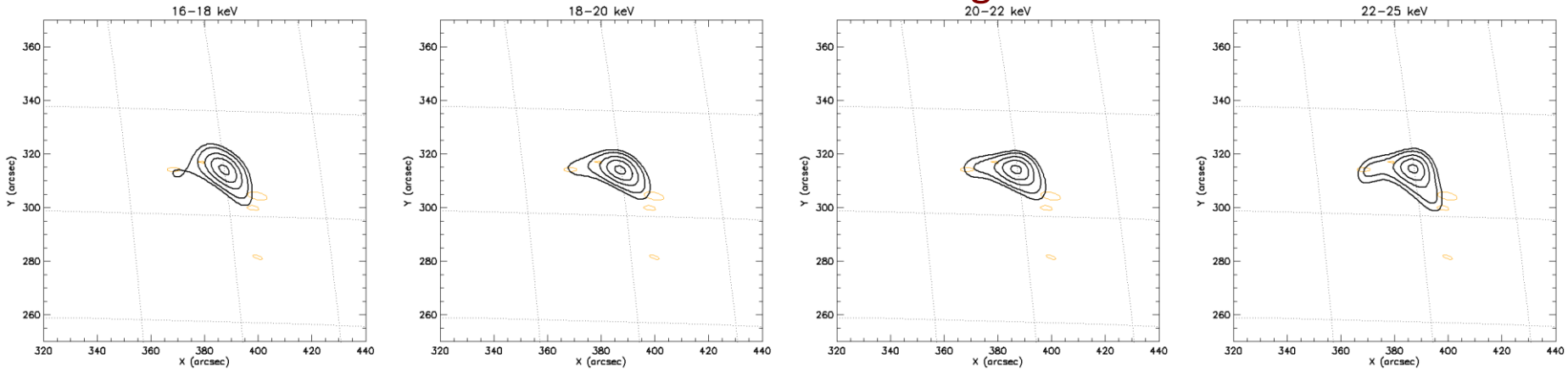

Photon images for the energy intervals shown (*top panels*), compared with the electron flux images corresponding to the regularized electron visibilities (*bottom panels*) in the same energy range. The 50% contour levels of the AIA images are plotted in orange, while the 25, 35, 55, 75, 95% contour levels of the reconstructed map are plotted in black. The maps are produced using the MEM-GE algorithm.

Results – May 7, 2021

Photon images

Electron flux images

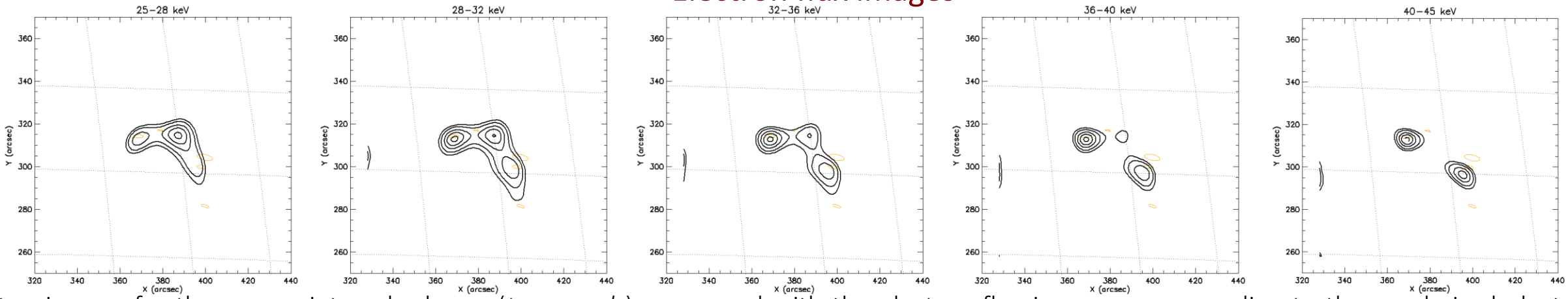

Photon images for the energy intervals shown (*top panels*), compared with the electron flux images corresponding to the regularized electron visibilities (*bottom panels*) in the same energy range. The 50% contour levels of the AIA images are plotted in orange, while the 25, 35, 55, 75, 95% contour levels of the reconstructed map are plotted in black. The maps are produced using the MEM-GE algorithm.

Results – May 7, 2021

Photon images

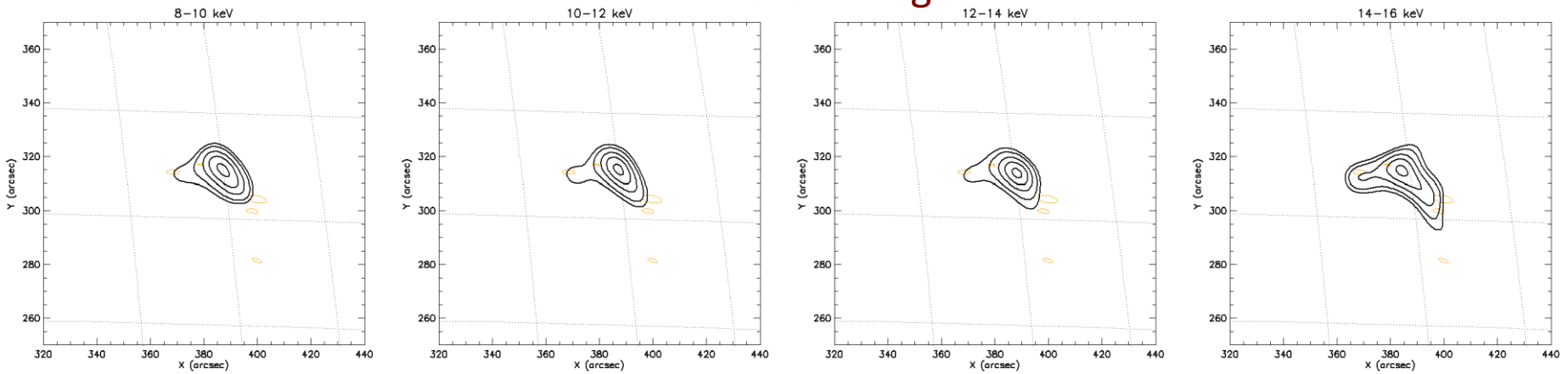

Regularized photon images

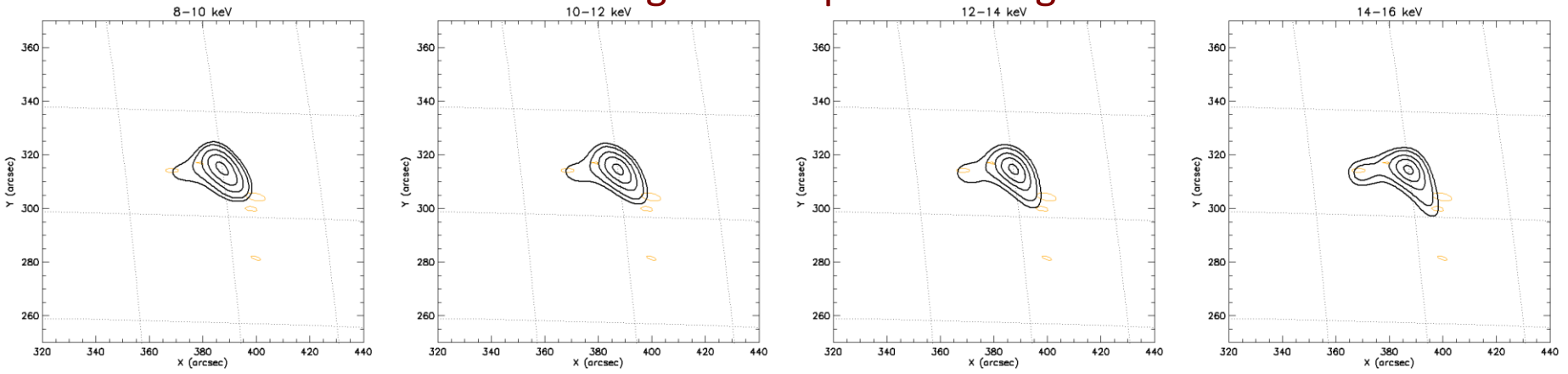

Photon images for the energy intervals shown (*top panels*), compared with the regularized photon-based images (*bottom panels*) in the same energy range. The 50% contour levels of the AIA images are plotted in orange, while the 25, 35, 55, 75, 95% contour levels of the reconstructed map are plotted in black. The maps are produced using the MEM-GE algorithm.

Results – May 7, 2021

Photon images

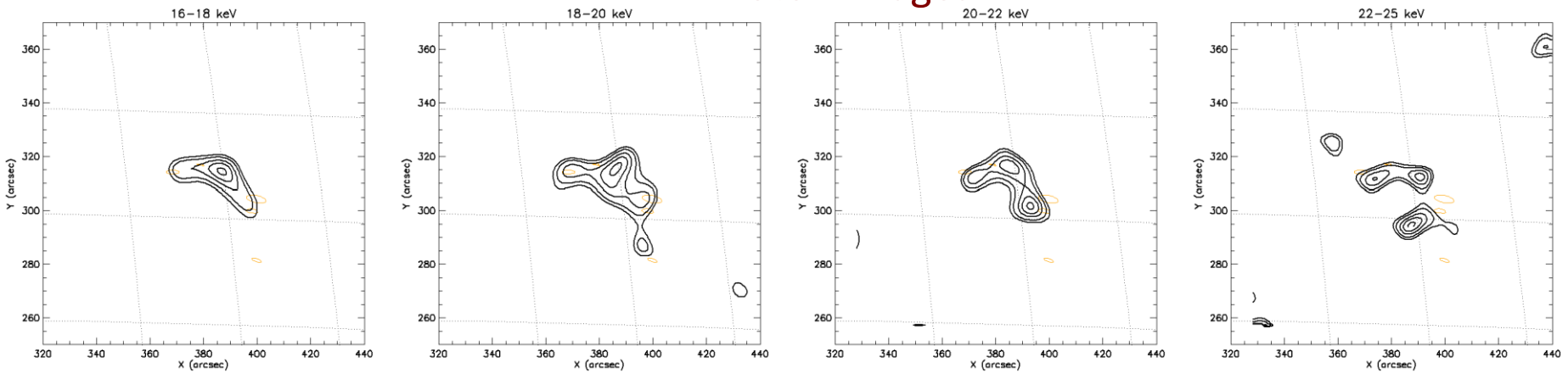

Regularized photon images

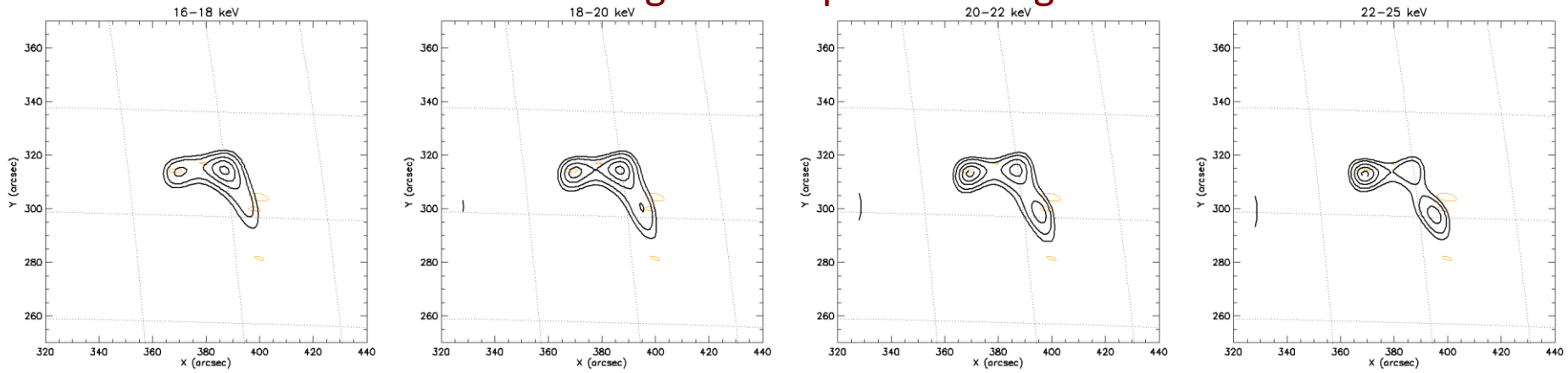

Photon images for the energy intervals shown (*top panels*), compared with the regularized photon-based images (*bottom panels*) in the same energy range. The 50% contour levels of the AIA images are plotted in orange, while the 25, 35, 55, 75, 95% contour levels of the reconstructed map are plotted in black. The maps are produced using the MEM-GE algorithm.

Results – May 7, 2021

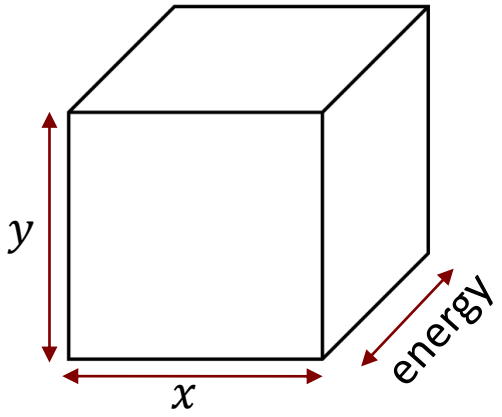

1. For each energy bin consider the total flux in the recovered map;
2. Consider the total flux as a function of the energy
3. Consider the flux spectrum provided by OSPEX

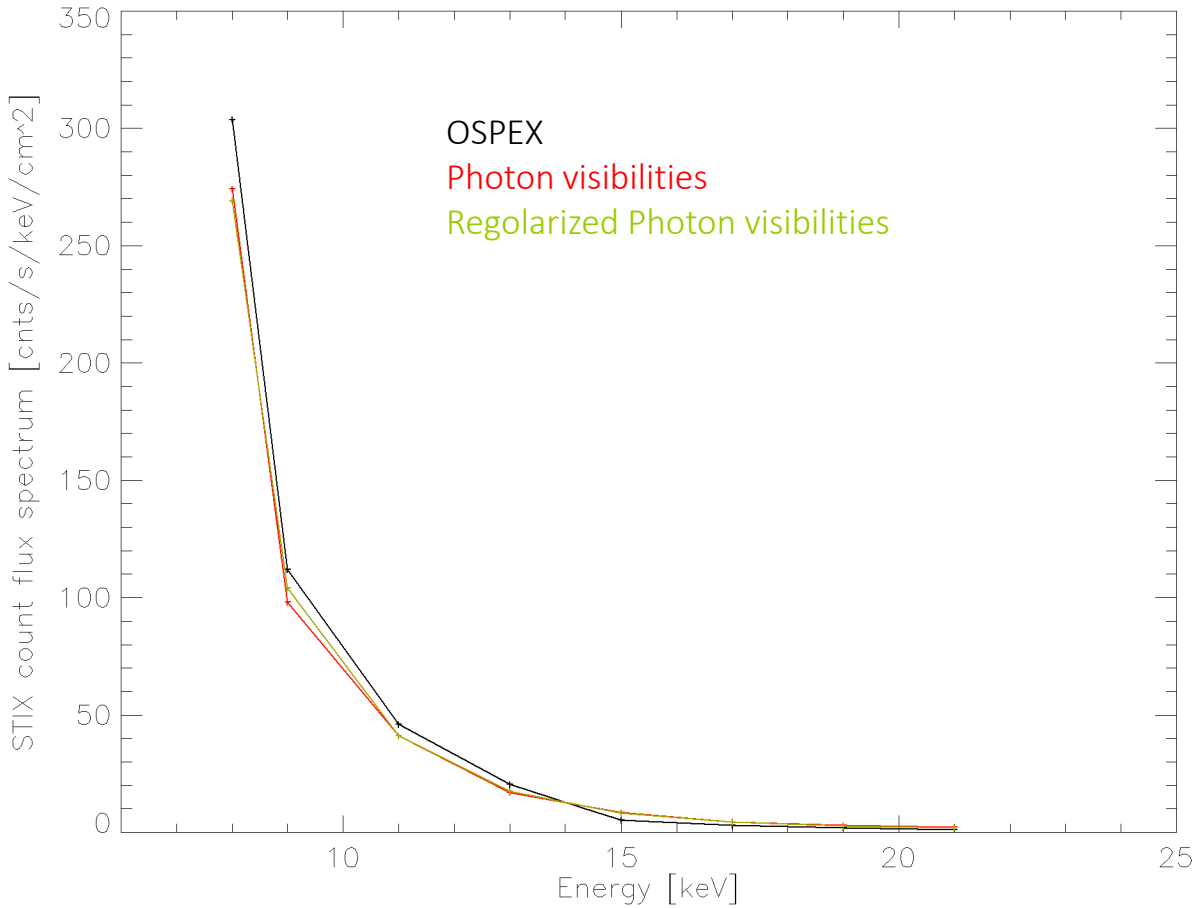

Total flux of the map reconstructed by MEM_GE , for May 7, 2021 event, considering photon visibilities (*in red*), regularized photon visibilities (*in green*), compared to OSPEX (*in black*).

Results – May 7, 2021

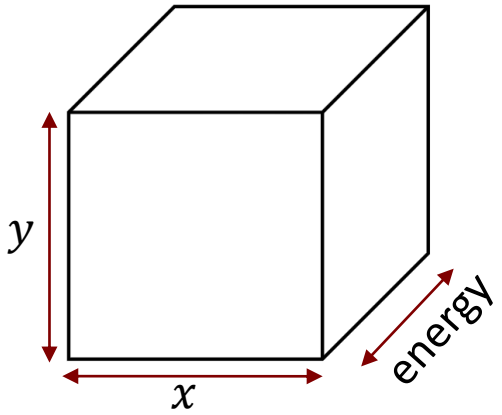

1. For each energy bin consider the total flux in the recovered map;
2. Consider the total flux as a function of the energy and fit with a power law
$$A\epsilon^{\gamma}$$
3. Consider the flux spectrum provided by OSPEX and fit it with a power law.

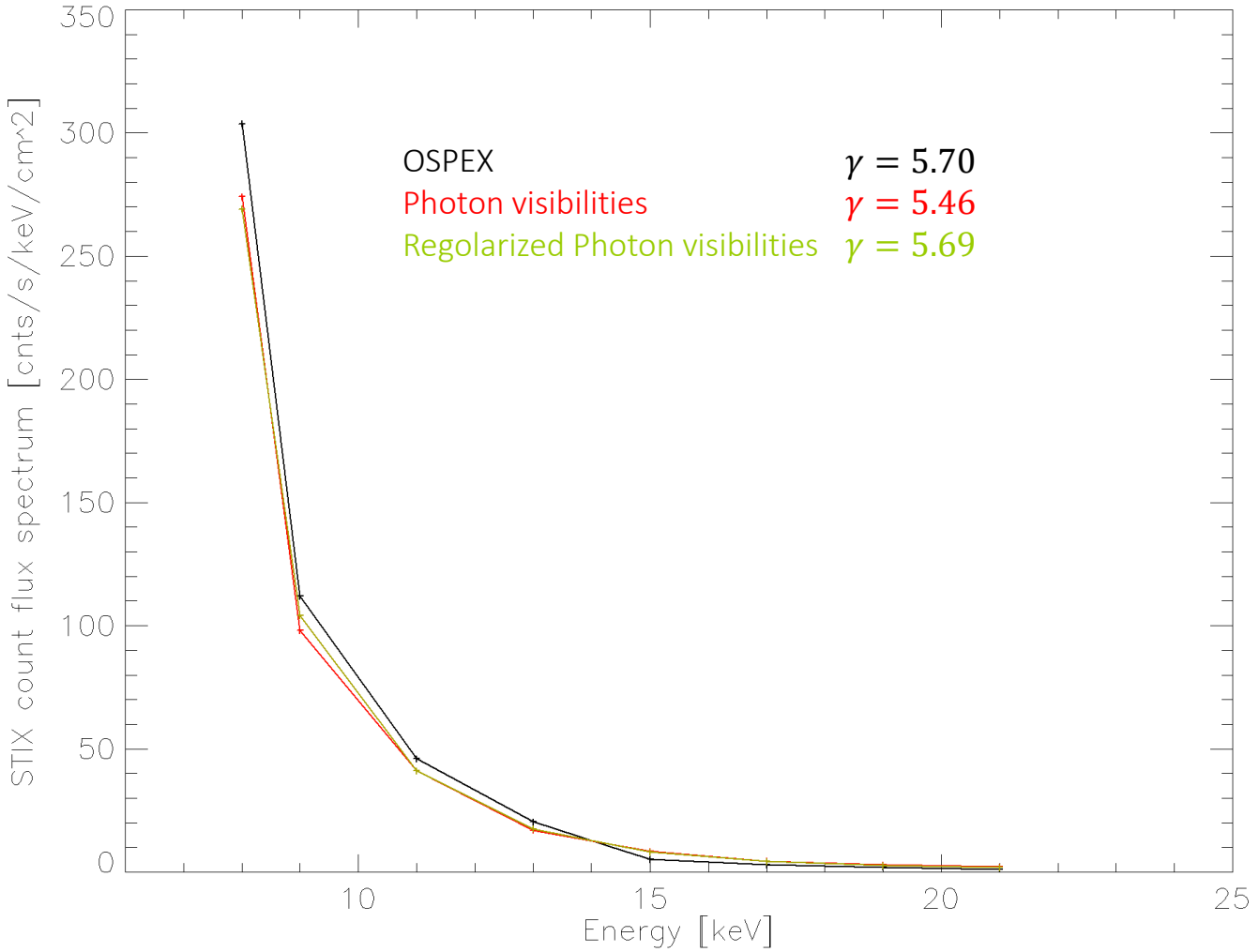

Results – May 7, 2021

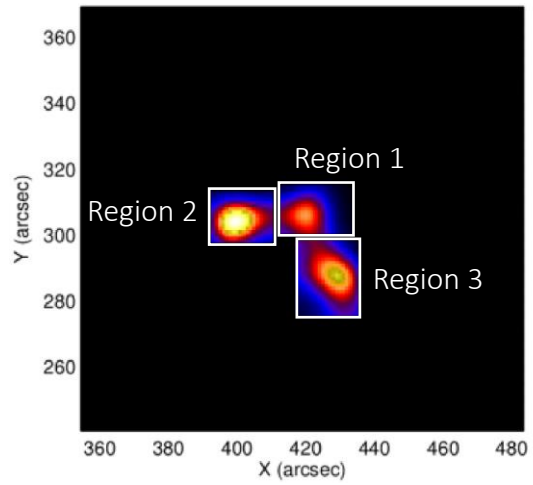

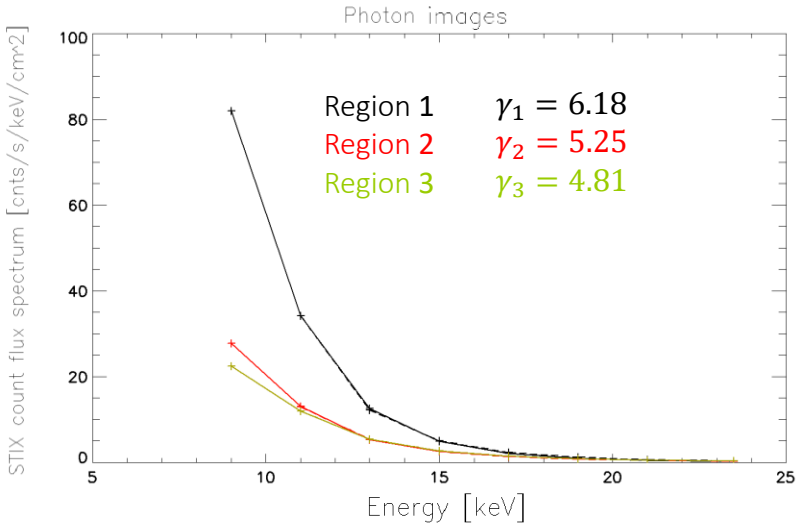

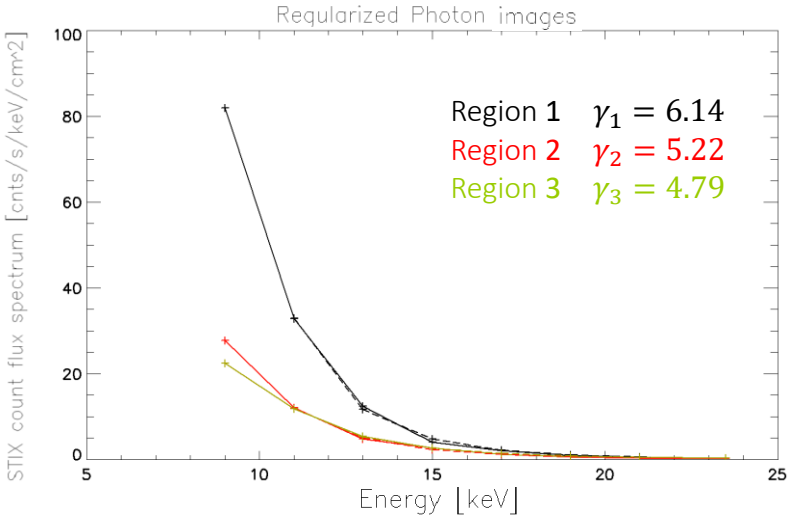

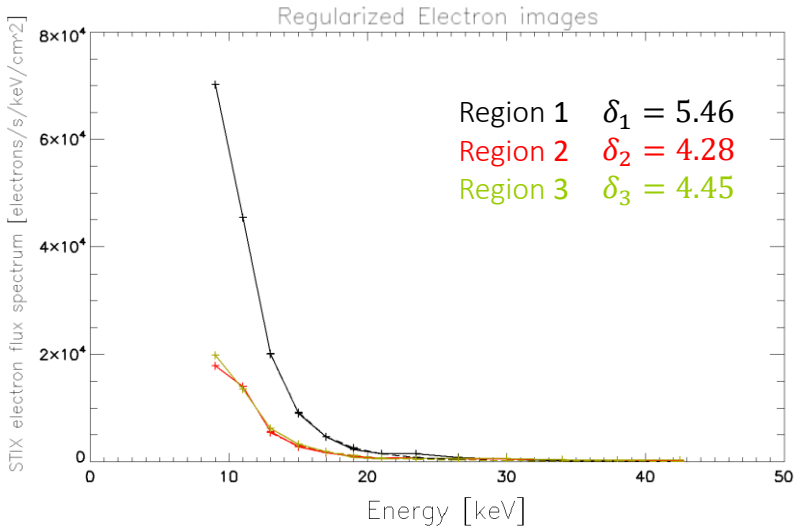

Top row: three selected subregions of the source (left panel) and STIX count flux spectrum and corresponding spectral index for the three selected subregions considering photon maps (right panel). Bottom row: STIX count flux spectrum and corresponding spectral index for the three selected subregions considering regularized photon maps (left panel) and the same in the case of electron flux spectrum (right panel).

Results – May 7, 2021

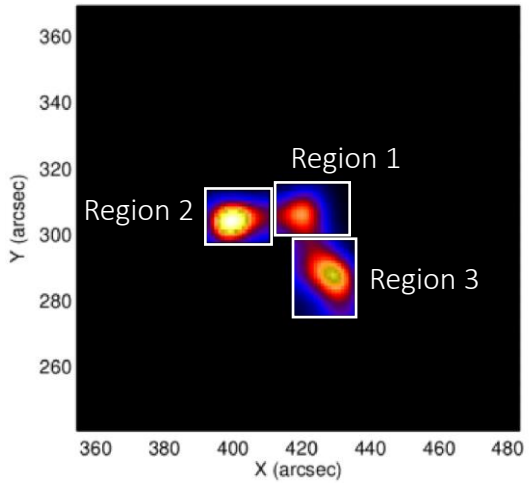

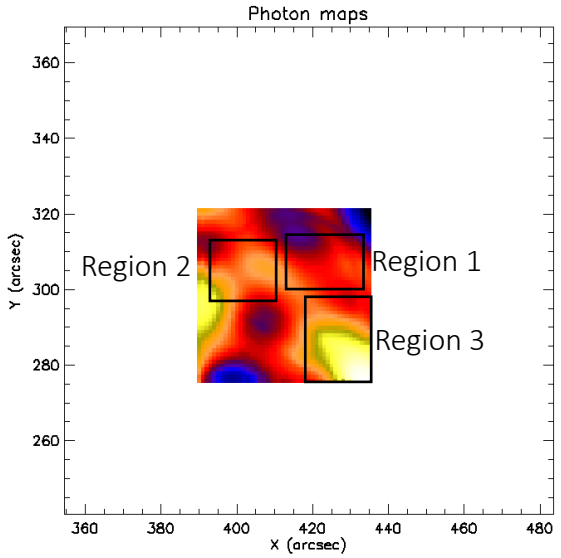

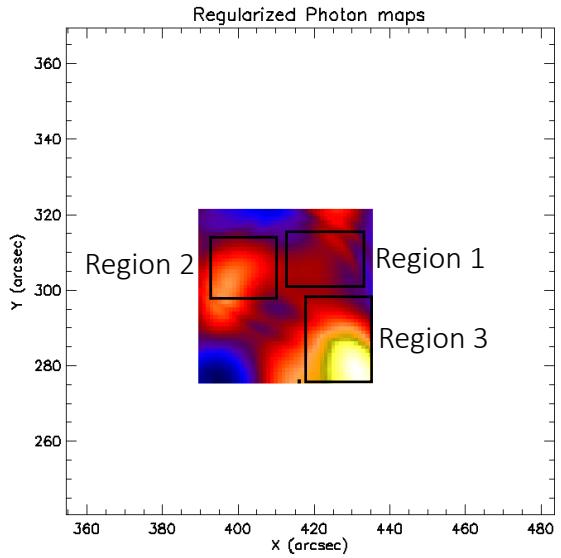

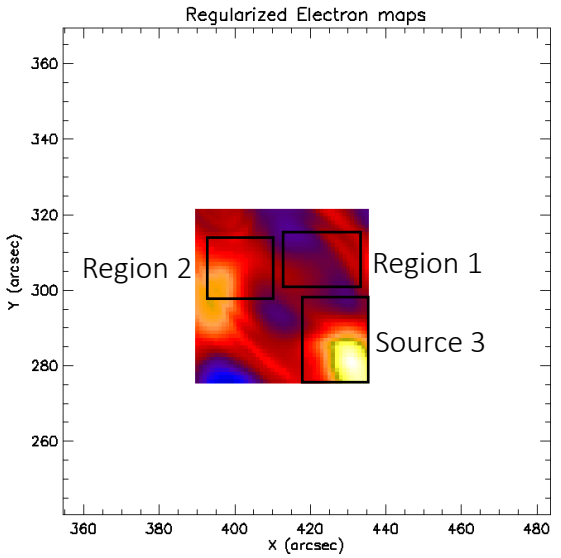

Left panel: three selected subregions of the source. Second, third and fourth panels show the pixel-wise spectral index for the three selected subregions considering photon maps, regularized photon maps and regularized electron maps, respectively.

	Region 1	Region 2	Region 3
Ph. maps	$\overline{\gamma_1} = 5.28$	$\overline{\gamma_2} = 4.51$	$\overline{\gamma_3} = 3.75$
Reg. Ph. Maps	$\overline{\gamma_1} = 5.25$	$\overline{\gamma_2} = 4.42$	$\overline{\gamma_3} = 3.47$
Reg. El. Maps	$\overline{\delta_1} = 3.93$	$\overline{\delta_2} = 3.02$	$\overline{\delta_3} = 2.67$

The table on the left shows the mean value of the spectral index in the three selected subregions of the source.

Results – November 11, 2022

Photon images

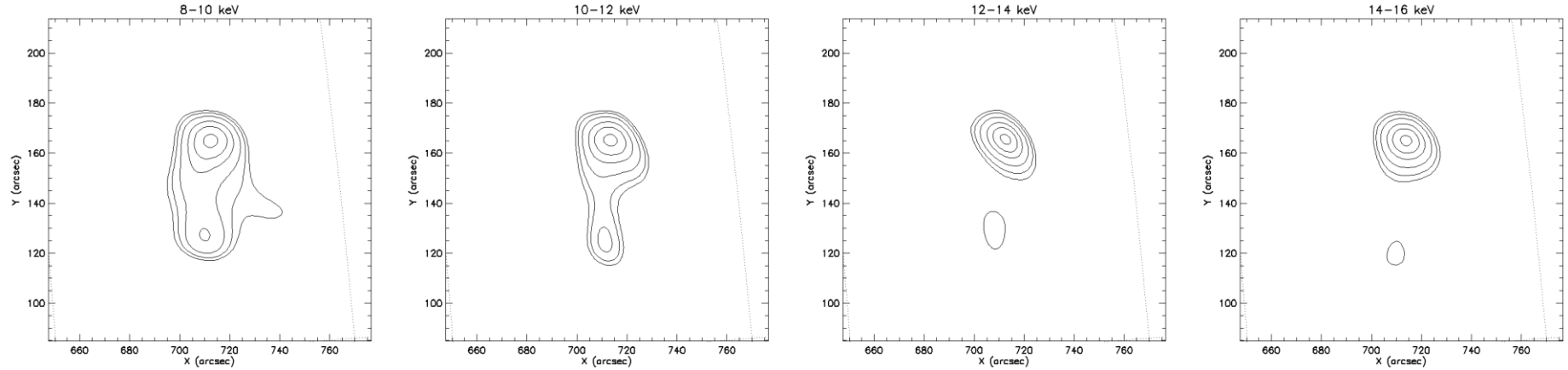

Electron flux images

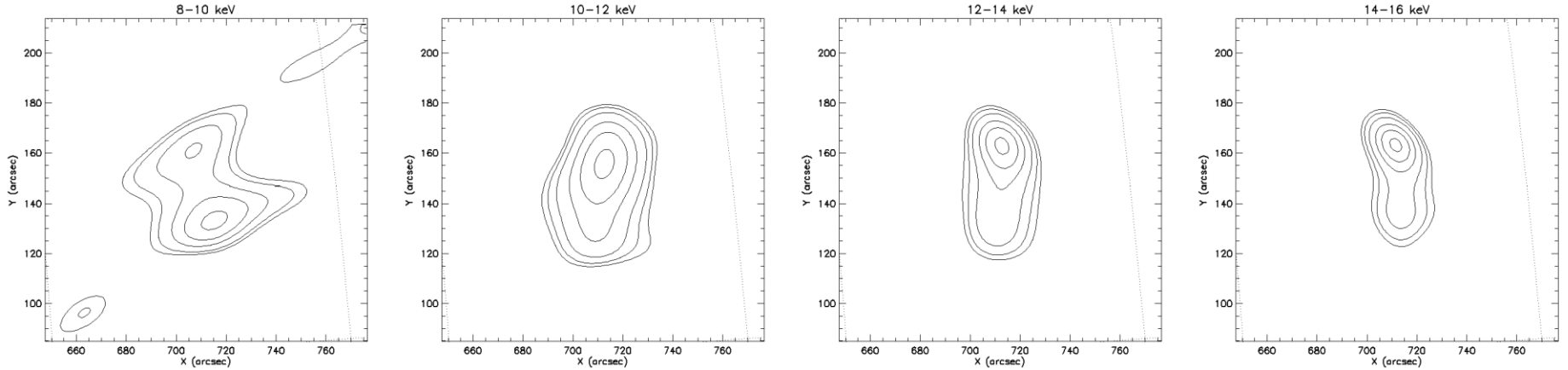

Photon images for the energy intervals shown (*top panels*), compared with the electron flux images corresponding to the regularized electron visibilities (*bottom panels*) in the same energy range. The 50% contour levels of the AIA images are plotted in orange, while the 25, 35, 55, 75, 95% contour levels of the reconstructed map are plotted in black. The maps are produced using the MEM-GE algorithm.

Results – November 11, 2022

Photon images

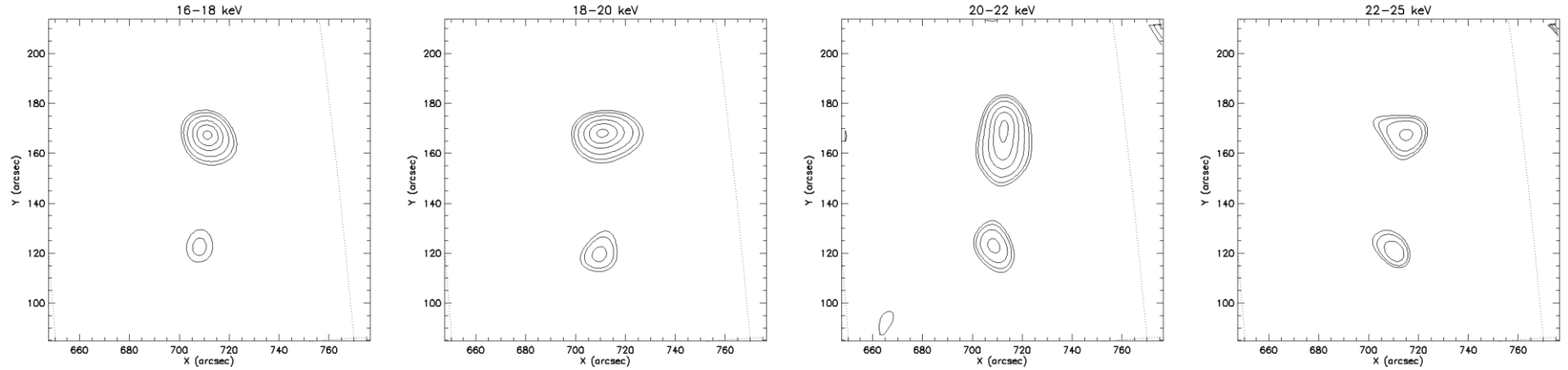

Electron flux images

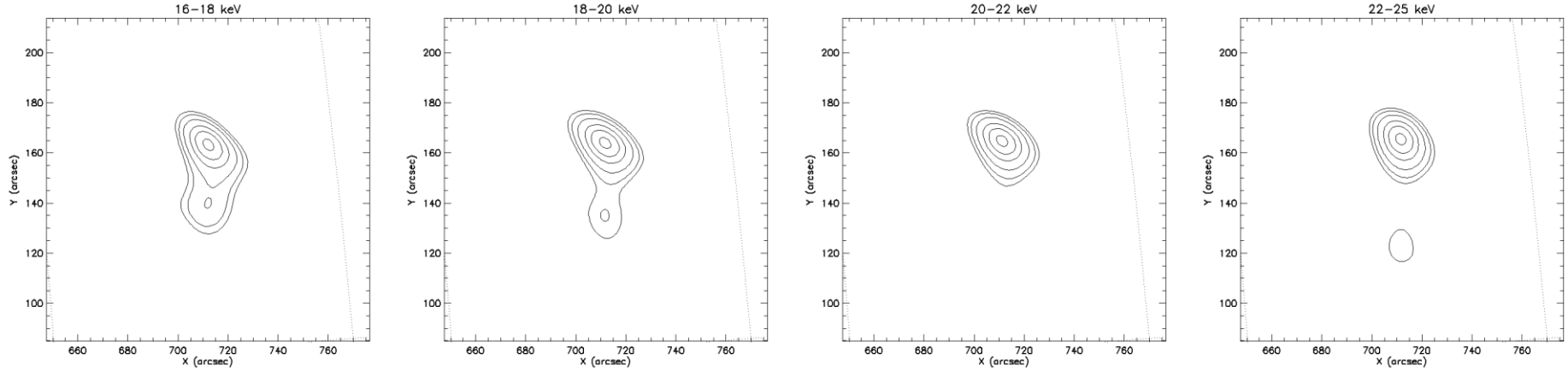

Photon images for the energy intervals shown (*top panels*), compared with the electron flux images corresponding to the regularized electron visibilities (*bottom panels*) in the same energy range. The 50% contour levels of the AIA images are plotted in orange, while the 25, 35, 55, 75, 95% contour levels of the reconstructed map are plotted in black. The maps are produced using the MEM-GE algorithm.

Results – November 11, 2022

Photon images

Electron flux images

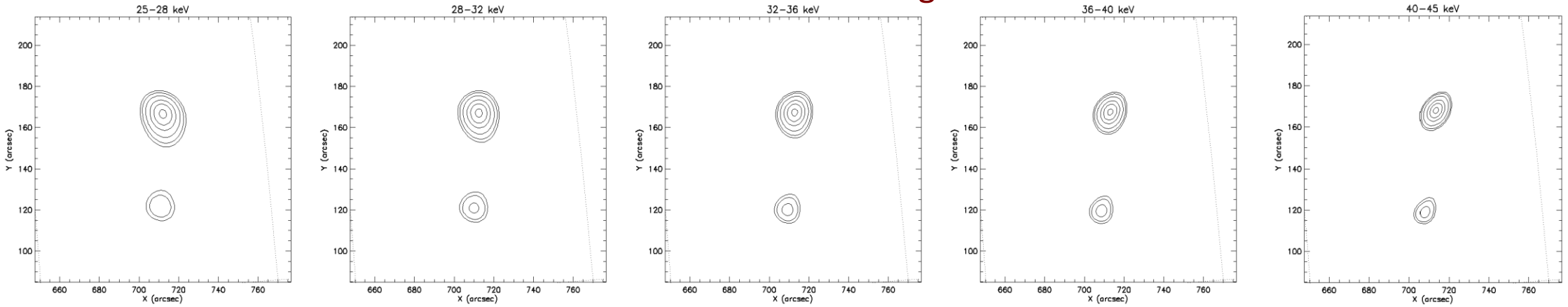

Photon images for the energy intervals shown (*top panels*), compared with the electron flux images corresponding to the regularized electron visibilities (*bottom panels*) in the same energy range. The 50% contour levels of the AIA images are plotted in orange, while the 25, 35, 55, 75, 95% contour levels of the reconstructed map are plotted in black. The maps are produced using the MEM-GE algorithm.

Results – November 11, 2022

Photon images

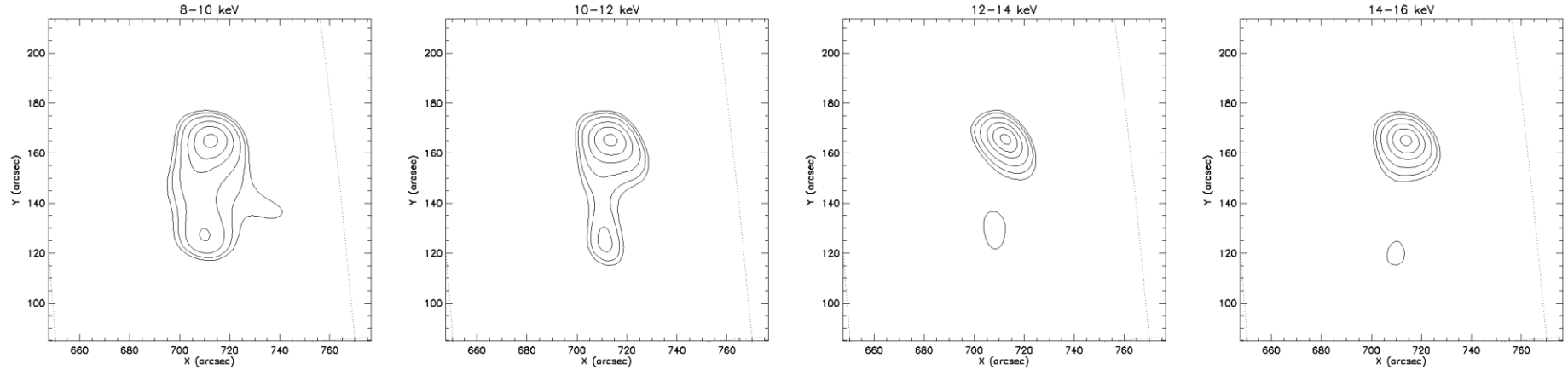

Regularized photon images

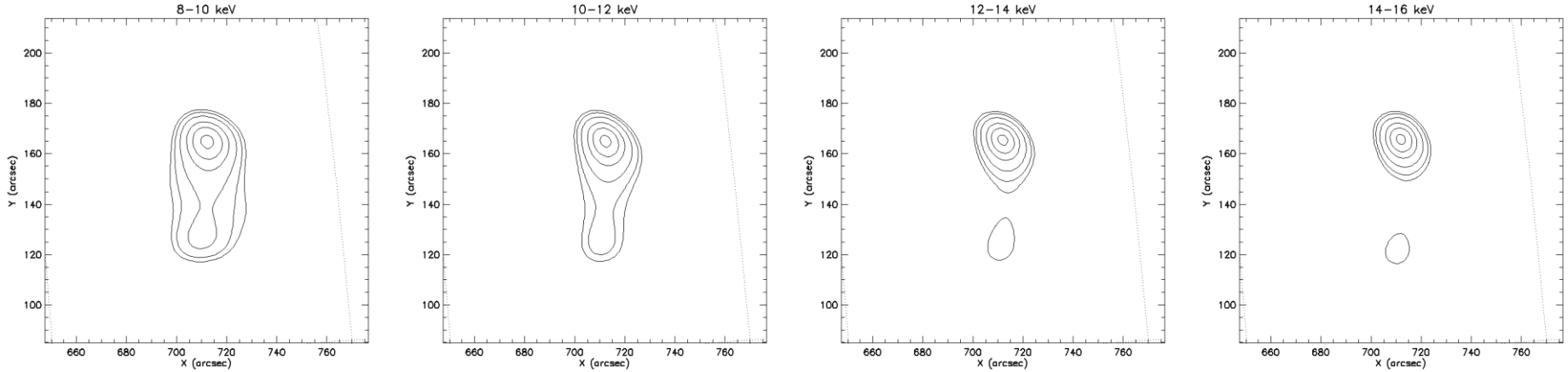

Photon images for the energy intervals shown (*top panels*), compared with the regularized photon-based images (*bottom panels*) in the same energy range. The 50% contour levels of the AIA images are plotted in orange, while the 25, 35, 55, 75, 95% contour levels of the reconstructed map are plotted in black. The maps are produced using the MEM-GE algorithm.

Results – November 11, 2022

Photon images

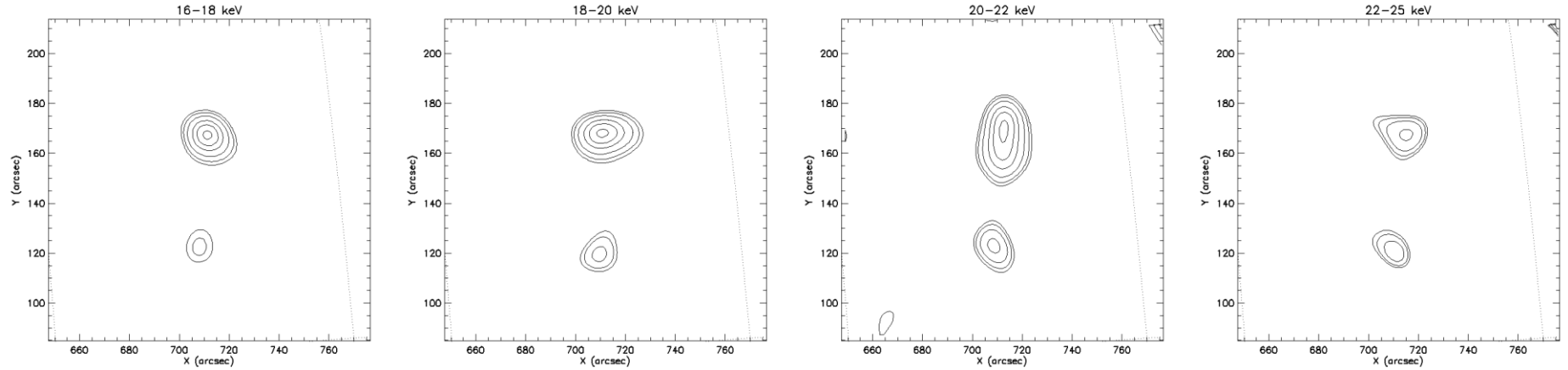

Regularized photon images

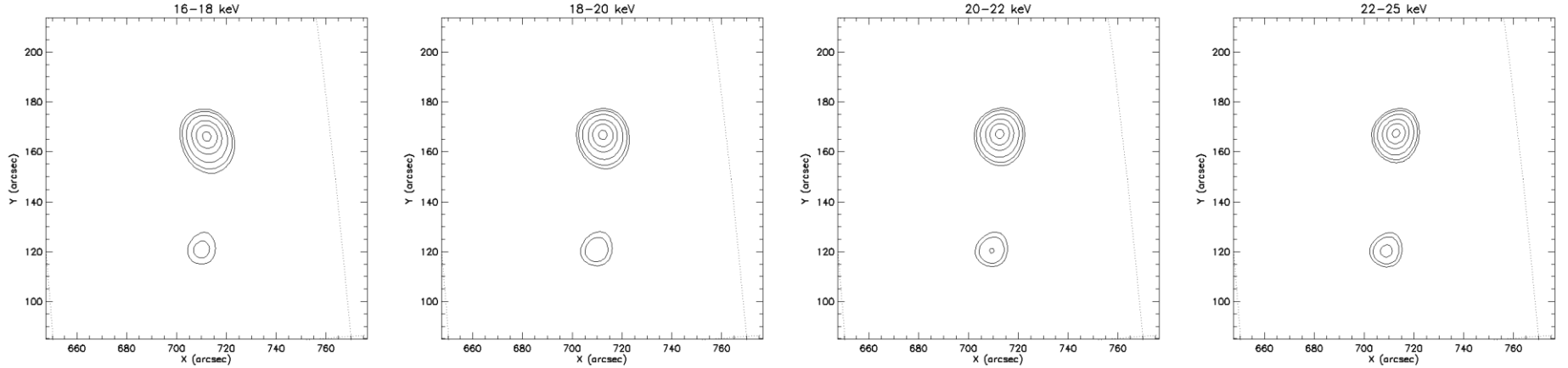

Photon images for the energy intervals shown (*top panels*), compared with the regularized photon-based images (*bottom panels*) in the same energy range. The 50% contour levels of the AIA images are plotted in orange, while the 25, 35, 55, 75, 95% contour levels of the reconstructed map are plotted in black. The maps are produced using the MEM-GE algorithm.

Results – November 11, 2022

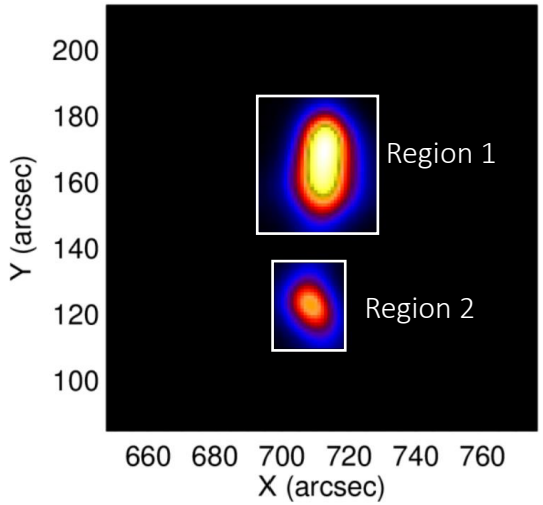

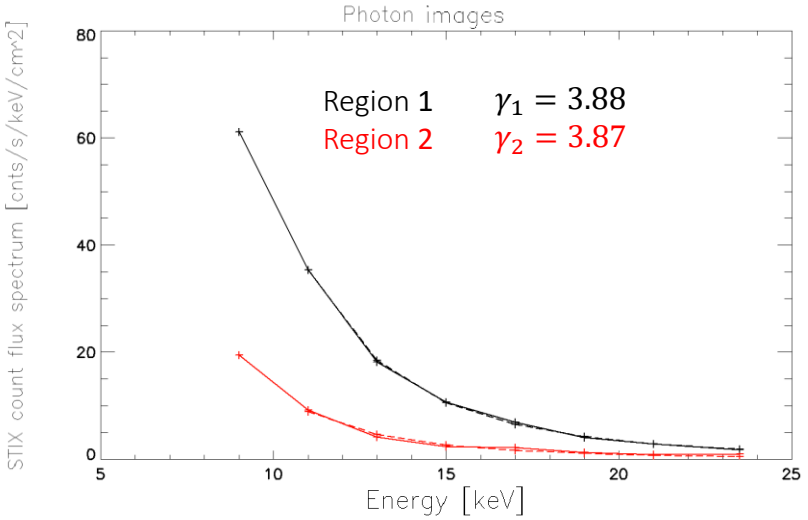

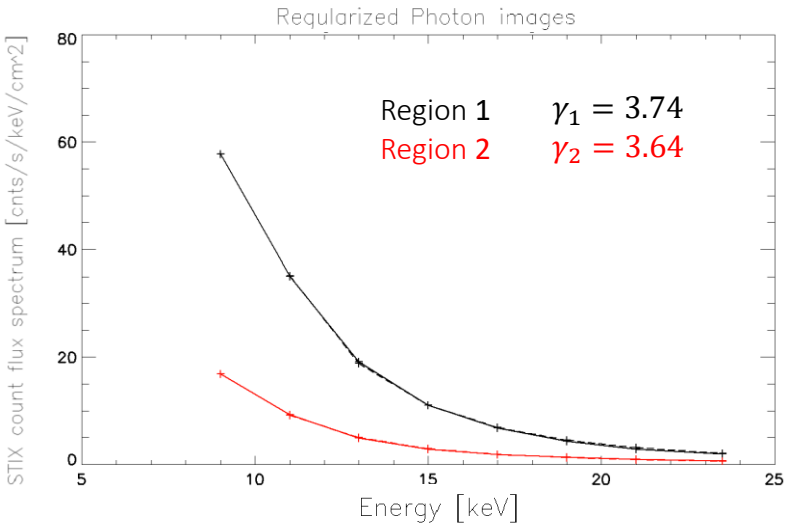

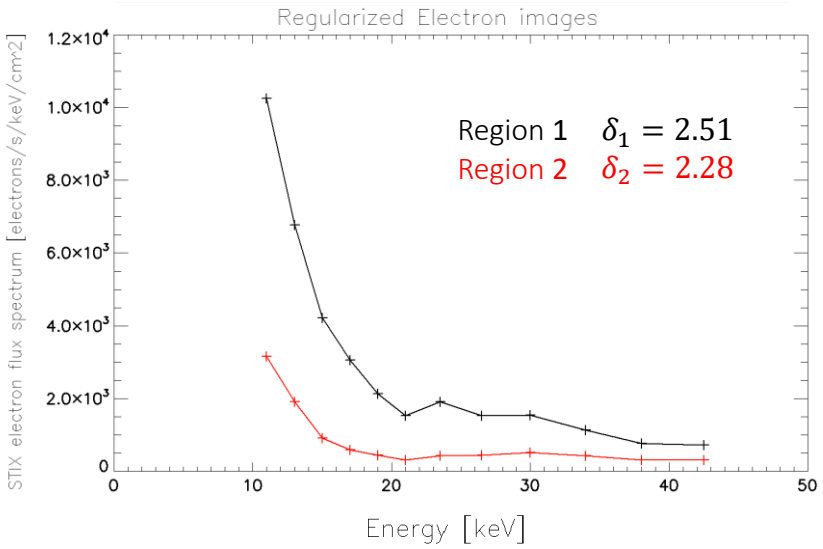

Top row: two selected subregions of the source (left panel) and STIX count flux spectrum and corresponding spectral index for the two selected subregions considering photon maps (right panel). Bottom row: STIX count flux spectrum and corresponding spectral index for the two selected subregions considering regularized photon maps (left panel) and the same in the case of electron flux spectrum (right panel).

Results – May 7, 2021

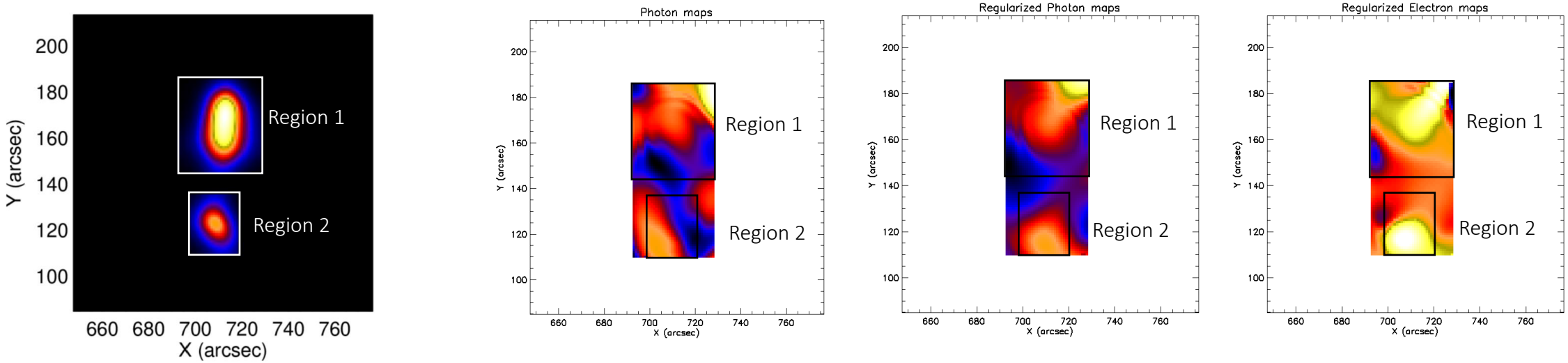

Left panel: two selected subregions of the source. Second, third and fourth panel show the pixel-wise spectral index for the two selected subregions considering photon maps, regularized photon maps and regularized electron maps, respectively.

	Region 1	Region 2
Ph. maps	$\overline{\gamma_1} = 3.30$	$\overline{\gamma_2} = 3.17$
Reg. ph. Maps	$\overline{\gamma_1} = 3.33$	$\overline{\gamma_2} = 3.13$
Reg. El. Maps	$\overline{\delta_1} = 2.11$	$\overline{\delta_2} = 1.79$

The table on the left shows the mean value of the spectral index in the two selected subregions of the source

Conclusions and future works

- ☑ We have described a new approach to solar hard X-ray imaging spectroscopy:
  - ☑ two-dimensional Fourier transforms of the image in the photon domain are transformed into Fourier transforms of the electron flux maps.
  - ☑ This tool also provides regularized photon visibilities corresponding to the regularized electron visibilities.
- ☑ We have proved inhomogeneity of the spectral index considering two flares observed by STIX.
- ❑ We are working on the time variability of the spectral index.
- ❑ We are working to take into account of both diagonal and non-diagonal terms of the DRM.
- ❑ We are testing this approach on more events to include the codes in SSW-IDL.

References

- Brown et al., *Fast spectral fitting of hard X-ray bremsstrahlung from truncated power-law electron spectra*, Astronomy and Astrophysics, (2008)
- Krucker et al., *The Spectrometer/Telescope for Imaging X-rays (STIX),* Astronomy and Astrophysics, (2020)
- Massa et al., *First Hard X-Ray Imaging Results by Solar Orbiter STIX*, Solar Physics, (2022)
- Massa et al., *MEM_GE: A New Maximum Entropy Method for Image Reconstruction from Solar X-Ray Visibilities*, The Astrophysical Journal, (2020)
- Massa et al., *STIX imaging I – Concept*, arxiv, (2023)
- Massone et al., *Regularized solution of the solar Bremsstrahlung inverse problem: model dependence and implementation issues*, Inverse Problems in Science and Engineering, (2004)
- Piana et al., *Electron flux spectral imaging of solar flares through regularized analysis of hard x-ray source visibilities,* The Astrophysical Journal, (2007)
- Piana et al., *Hard X-rays imaging of Solar Flares*, Springer, (2022)
- Prato et al., *A Regularized Visibility-Based Approach to Astronomical Imaging Spectroscopy*, SIAM Journal on Imaging Sciences, (2009)

THANK YOU FOR THE ATTENTION!

Università di Genova
DIMA | Dipartimento di Matematica
MIDA group

n|w

Università di Genova